New Journal of Physics

The open access journal at the forefront of physics

CrossMark

PAPER

Fragmented condensation in Bose–Hubbard trimers with tunable tunnelling

A Gallemí[1,2], M Guilleumas[1,2], J Martorell[1], R Mayol[1,2], A Polls[1,3] and B Juliá-Díaz[1,3,4]

1 Departament d'Estructura i Constituents de la Matèria, Facultat de Física, Universitat de Barcelona, E-08028 Barcelona, Spain
2 Institut de Nanociència i Nanotecnologia de la Universitat de Barcelona (IN² UB), E-08028 Barcelona, Spain
3 Institut de Ciències del Cosmos, Universitat de Barcelona, ICC-UB, Martí i Franquès 1, E-08028 Barcelona, Spain
4 ICFO-Institut de Ciències Fotòniques, Parc Mediterrani de la Tecnologia, E-08860 Barcelona, Spain

E-mail: gallemi@ecm.ub.edu

Abstract

We consider a Bose–Hubbard (BH) trimer, i.e. an ultracold Bose gas populating three quantum states. The latter can be either different sites of a triple-well potential or three internal states of the atoms. The bosons can tunnel between different states with variable tunnelling strength between two of them. This will allow us to study; (i) different geometrical configurations, i.e. from a closed triangle to three aligned wells and (ii) a triangular configuration with a π-phase, i.e. by setting one of the tunnellings negative. By solving the corresponding three-site BH Hamiltonian we obtain the ground state of the system as a function of the trap topology. We characterize the different ground states by means of the coherence and entanglement properties. For small repulsive interactions, fragmented condensates are found for the π-phase case. These are found to be robust against small variations of the tunnelling in the small interaction regime. A low-energy effective many-body Hamiltonian restricted to the degenerate manifold provides a compelling description of the π-phase degeneration and explains the low-energy spectrum as excitations of discrete semifluxon states.

1. Introduction

It is well known that bosons at sufficiently low temperatures tend to form Bose–Einstein condensates (BECs), which essentially consist on the macroscopic population of a single-particle state [1]. In absence of interactions, the macroscopically occupied state is the lowest energy state of the single-particle Hamiltonian. When the interatomic interactions are taken into account, and for sufficiently large number of atoms, the main effect is a broadening of the single-particle state, which can be accounted for by a mean-field Gross–Pitaevskii description. In the Onsager–Penrose picture, in a BEC there is only one eigenvalue of the one-body density matrix which is of the order of the total number of particles. This is the largest eigenvalue and is termed the 'condensed fraction'.

In contrast, an interesting scenario appears when, in absence of interactions, the lowest single-particle states are degenerate. In this case, the many-body ground state may get fragmented [2], as naively the atoms have no reason to condense in only one of the degenerate single-particle states. This implies that a finite number of eigenvalues of the single-particle density matrix are of order of the total number of atoms.

In [2] the authors describe three notable physical examples which produce fragmented condensates, e.g. the highly correlated regime in ultracold gases subjected to synthetic gauge fields, the two-site Hubbard model and the ground state of a spinor condensate in absence of quadratic Zeeman terms. In the first two cases, interactions need to dominate over tunnelling terms in order to get fragmentation. For instance, for atoms in the double-well it is in the strongly repulsive regime that the condensate fragments in two parts, with half the atoms populating each well. By increasing the potential barrier between the wells, the system enters into the Fock regime (interaction energy dominating over the tunnelling) and fragments in two BECs of equal number of particles. This has been realized experimentally [3–6]. Notably, the quantum many-body correlations present in

fragmented states can find applications in the field of quantum metrology to improve precision measurements [5], and hold promise of being useful in near future technological applications [7].

It is desirable to pin down quantum many-body systems which feature fragmentation even at the single-particle level without explicit spatial separation. In this article we consider a minimal system which fulfills this, and which therefore has fragmented ground states both in absence of atom–atom interactions or for small ones. We consider N identical bosons populating three single-particle states. The bosons are assumed to be able to tunnel between the different states. There are two options that are available with current techniques. The first one would be to trap the atoms in a triple-well potential, with fully connected sites as in [8–11], or aligned [12]. In this case, the three quantum states are the three eigenstates of the single-particle Hamiltonian, which are thus spatially localized. The properties of such triple-well potentials have been studied previously exploring the many-body properties of symmetric trimers [12–14], of vortex states in symmetric trimers [10, 11, 15] and the effect of dipolar interactions in the system [16–20]. A second option is to investigate three different internal states of the boson as single-particle states, with the whole cloud being trapped on the same harmonic potential. Transitions among the three internal states can be induced by means of Rabi coupling. In this case, the three quantum states are not spatially localized. These two cases may be referred to as external or internal, three-mode systems.

In previous studies, the coupling between the different modes is provided by the quantum tunnelling between the spatially localized modes. This has hindered the exploration of the regime we discuss in the present article. The key idea is to consider systems where tunnelling can be detuned [21] and particularly profit from the recent advances in producing phase dependent tunnelling terms. Namely, we will study triangular setups in which one of the tunnelling terms can be taken negative. This means that a particle tunnelling from that site to the next one acquires a phase of π. Thus, we consider cases in which a particle acquires either 0 or π phase when tunnelling around the triangle in absence of interactions. For external modal configurations, an external shaking of the system along one direction effectively results in a dressed tunnelling term whose sign can be switched from positive (standard) values to negative (π-phase tunnelling) [22]. More recently, a deep laser dip in the centre of a junction has been proposed in [23] to engineer π-phase tunnelling. In the internal case a phase-dependent tunnelling can be obtained as in [24]. Our proposal allows one to study a variety of regimes by just modifying the tunnelling properties of one link. In particular, in certain cases, we recover the known physics for 0- or π-flux symmetric trimers studied in [9, 10, 15]. In the π-flux case, our particular implementation will be easily interpreted in terms of semifluxon states (fractional vortices) [25].

This paper is organized as follows. In section 2, we present the three-mode Bose–Hubbard (BH) Hamiltonian, discussing the single-particle case and briefly recalling the many-body magnitudes that are used to characterize the system. Section 3 is devoted to analyse the role played by interactions for different configurations, and the entanglement and correlation properties of the system. Finally, in section 4 we summarize our conclusions and provide possible implications for future experiments.

2. Three-mode BH Hamiltonian

We assume N ultracold bosons populating three quantum states. As discussed above, they can be different sites, e.g. an ultracold gas confined in a triple-well potential (see for instance [18] for a possible explicit expression of the potential), or three internal states of the atoms. For the time being, we will restrict our system to the former case. We consider tunnelling terms between the three sites, and a tunable rate between two of them. This tunable rate will allow us to explore colinear configurations, closed ones, and also configurations with π phase. Besides the tunnelling, the atoms interact via s-wave contact interactions. This interaction is assumed to be the same between all atoms, which is straightforward in the external case, as there is only one kind of atoms, but would require some tuning in the internal case depending on the species. The three-mode BH Hamiltonian we consider is thus,

$$\hat{\mathcal{H}} = -J\left(\hat{a}_1^\dagger \hat{a}_2 + \gamma\,\hat{a}_1^\dagger \hat{a}_3 + \hat{a}_2^\dagger \hat{a}_3 + \text{h.c.}\right) + \frac{U}{2}\sum_{i=1}^{3}\hat{n}_i\left(\hat{n}_i - 1\right),\tag{1}$$

where $\hat{a}_i$ ($\hat{a}_i^\dagger$) are the bosonic annihilation (creation) operators for site i fulfilling canonical commutation relations, and $\hat{n}_i = \hat{a}_i^\dagger \hat{a}_i$ is the particle number operator on the ith site. J is the tunnelling coefficient between sites 1–2, and 2–3, and U is the atom–atom on-site interaction that can be repulsive $U > 0$ or attractive $U < 0$. In our study, sites 1 and 3 are always equivalent with respect to site 2, and the tunnelling between sites 1–3 depends on the particular configuration through the parameter γ.

Figure 1 shows schematically the triple-well potentials we have addressed. When $\gamma = 0$, no tunnelling exists between sites 1 and 3, which corresponds to an aligned triple-well configuration. When $0 < \gamma < 1$, sites 1 and 3 are connected but the tunnelling between 1 and 2 (and 2–3 as well) is larger. In contrast, when $\gamma = 1$, the three sites are fully equivalent with the same tunnelling rate among them, which can be geometrically interpreted as arranged in an equilateral triangular potential. We will go beyond this symmetric configuration, when $\gamma > 1$, by
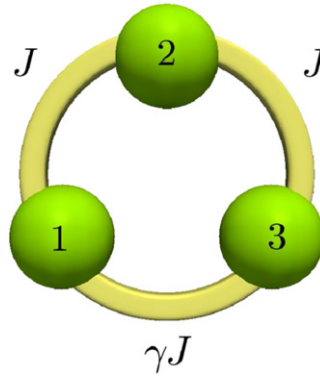
Figure 1. Schematic depiction of the system under study. We consider a gas of bosons which can populate three different modes, depicted as green balls. Bosons are allowed to tunnel between the modes. The tunnelling between modes 1 and 3 is taken to be tunable through the parameter γ. For $\gamma = 0$ the three sites are aligned and the geometry is essentially one dimensional. For $\gamma > 0$ we have a triangular configuration, which for $\gamma = 1$ is equilateral. In the limit of $\gamma \gg 1$ the system is similar to a two-mode one. For $\gamma < 0$ we have π-phase tunnelling between sites 1 and 3.

increasing the tunnelling rate between sites 1 and 3 with respect to 1–2 (and 2–3), up to $\gamma = 2$ and we will also consider negative values of γ. These values of γ can be engineered by lattice shaking along the direction of sites 1 and 3 [22]. In the particular case of $\gamma = -1$, the many-body Hamiltonian of equation (1) can be mapped by a local gauge transformation onto the Hamiltonian of a rotating trimer with a phase gradient of $\pi/3$ [10, 13, 15]. In both cases, the (gauge independent) flux is equal to π. Our system provides a different experimental way of producing the same physics, and an alternative route, by varying γ, to engineer fragmented many-body states.

The Hamiltonian of equation (1) can also be reproduced with a three-component (spinorial, isotopic or atomic) BEC mixture trapped on a single harmonic oscillator with suitable Rabi coupling between the levels (which corresponds to the tunnelling terms).

Our study will concentrate mostly on the repulsive interaction case, which is more prone to be experimentally explored with current setups. We will also discuss briefly the attractive interaction case. In the latter even small asymmetries in the external trapping potentials will eventually have a large impact on the properties of the ground state [26]. Thus, we will introduce small symmetry breaking terms, compared to both the tunnelling and interaction, to consider situations closer to experimental ones and also to control numerically the degeneracies in the problem. We have added the biases between sites 1–3 and 2–3, ϵ_{13} and ϵ_{23}, respectively. The considered Hamiltonian now reads:

$$\hat{\mathcal{H}}' = \hat{\mathcal{H}} + \epsilon_{13}\left(\hat{n}_1 - \hat{n}_3\right) + \epsilon_{23}\left(\hat{n}_2 - \hat{n}_3\right). \tag{2}$$
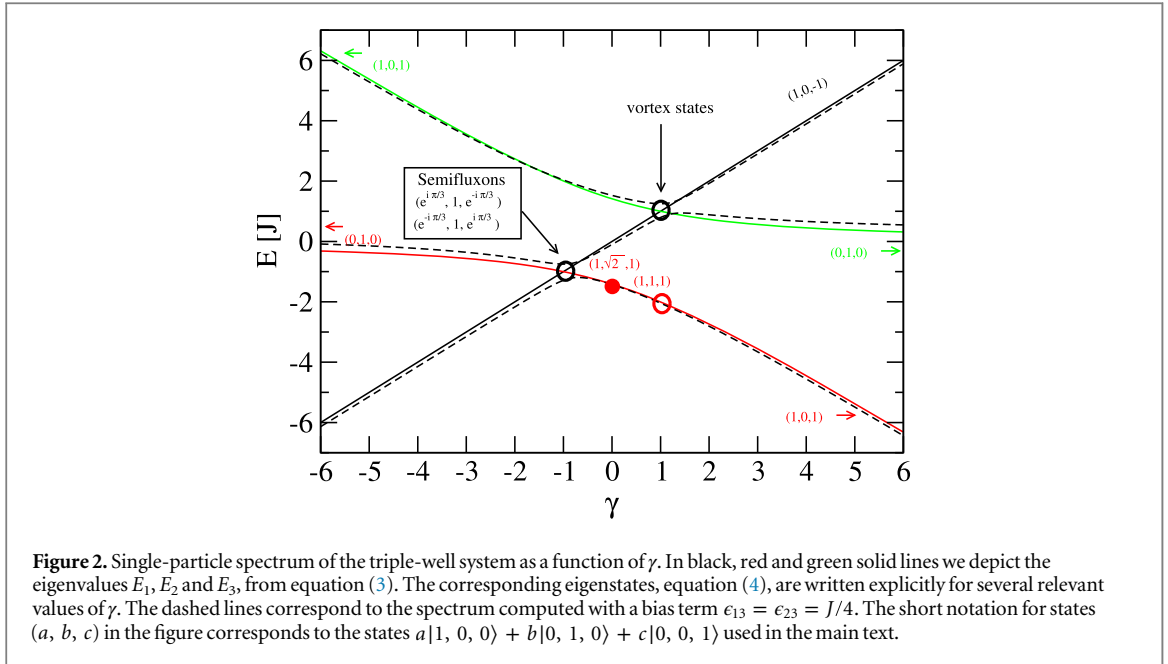
2.1. Single-particle case

In this section we solve the single-particle case for any value of the tunable tunnelling link γJ. In our calculation we will keep the tunnelling parameter fixed $J/h = 1$ Hz, since it essentially sets the overall energy scale.

The triple-well configuration we have chosen is intended to remark first, the role played by the topology of the configuration, going from a disconnected chain ($\gamma = 0$) to an essentially double-well system at $\gamma \to \infty$, through a connected equilateral triangle at $\gamma = 1$. It is worth emphasizing that we do so by varying the tunnelling strength between sites 1 and 3 and not by, for instance, adding sizeable bias terms to the Hamiltonian, which would indeed also break the symmetry between the three sites. The second important point, is that we consider π-phase tunnelling between the two wing sites ($\gamma < 0$), which will indeed have dramatic consequences on the many-body properties of the system.

2.1.1. Unbiased single-particle case

The single-particle case can be readily solved. The eigenvalues of the Hamiltonian (1) with $U = 0$ are,

$$E_1 = \gamma J,$$

$$E_2 = \frac{J}{2}\left(-\gamma - \sqrt{8 + \gamma^2}\right),$$

$$E_3 = \frac{J}{2}\left(-\gamma + \sqrt{8 + \gamma^2}\right), \tag{3}$$

Figure 2. Single-particle spectrum of the triple-well system as a function of γ. In black, red and green solid lines we depict the eigenvalues E_1, E_2 and E_3, from equation (3). The corresponding eigenstates, equation (4), are written explicitly for several relevant values of γ. The dashed lines correspond to the spectrum computed with a bias term $\epsilon_{13} = \epsilon_{23} = J/4$. The short notation for states (a, b, c) in the figure corresponds to the states $a|1, 0, 0\rangle + b|0, 1, 0\rangle + c|0, 0, 1\rangle$ used in the main text.

and the corresponding unnormalized eigenvectors are:

$$\left|\psi_1\right\rangle = \frac{1}{\sqrt{2}}\left(|1, 0, 0\rangle - |0, 0, 1\rangle\right),$$

$$\left|\psi_2\right\rangle = |1, 0, 0\rangle + \frac{4 - \gamma^2 + \gamma\sqrt{8 + \gamma^2}}{\sqrt{8 + \gamma^2} + 3\gamma}\,|0, 1, 0\rangle + |0, 0, 1\rangle,$$

$$\left|\psi_3\right\rangle = |1, 0, 0\rangle + \frac{-4 + \gamma^2 + \gamma\sqrt{8 + \gamma^2}}{\sqrt{8 + \gamma^2} - 3\gamma}\,|0, 1, 0\rangle + |0, 0, 1\rangle. \tag{4}$$

The single-particle spectrum, see figure 2, has some interesting features. First, there is one eigenvector that is independent of γ, $|\psi_1\rangle$. This state does not involve site 2, and its energy is proportional to the coupling between sites 1 and 3. For $\gamma = 0$, which corresponds to an aligned configuration, the ground state is $|\psi_2\rangle_{\gamma=0} = (1/2)\left(|1, 0, 0\rangle + \sqrt{2}\,|0, 1, 0\rangle + |0, 0, 1\rangle\right)$, which has an excess of particles in site 2.

As γ is increased, the equilateral triangular configuration is reached for $\gamma = 1$. This case has been studied thoroughly in [11, 29]. The ground state is $|\psi_2\rangle_{\gamma=1} = (1/\sqrt{3})(|1, 0, 0\rangle + |0, 1, 0\rangle + |0, 0, 1\rangle)$ and there are two excited degenerate single-particle states that correspond to vortex states, with 2π-flux and clockwise and counter-clockwise rotation:

$$\left|\psi_{v1}\right\rangle = \frac{1}{\sqrt{3}}\left(|1, 0, 0\rangle + e^{i\frac{2\pi}{3}}|0, 1, 0\rangle + e^{i\frac{4\pi}{3}}|0, 0, 1\rangle\right),$$

$$\left|\psi_{v2}\right\rangle = \frac{1}{\sqrt{3}}\left(|1, 0, 0\rangle + e^{-i\frac{2\pi}{3}}|0, 1, 0\rangle + e^{-i\frac{4\pi}{3}}|0, 0, 1\rangle\right). \tag{5}$$

Notice that these two states are linear combinations of

$$\left|\psi_1\right\rangle = \frac{1}{\sqrt{2}}\left(e^{-i\frac{\pi}{6}}\left|\psi_{v1}\right\rangle + e^{i\frac{\pi}{6}}\left|\psi_{v2}\right\rangle\right) \qquad \text{and}$$

$$\left|\psi_3\right\rangle_{\gamma=1} = \frac{1}{\sqrt{6}}\left(|1, 0, 0\rangle - 2|0, 1, 0\rangle + |0, 0, 1\rangle\right)$$

$$= \frac{1}{\sqrt{2}}\left(e^{i\frac{\pi}{3}}\left|\psi_{v1}\right\rangle + e^{-i\frac{\pi}{3}}\left|\psi_{v2}\right\rangle\right). \tag{6}$$

Further increasing γ, sites 1 and 3 get further connected and the physics decouples them from site 2. The ground state for $\gamma \to \infty$ is $|\psi_2\rangle_{\gamma\to\infty} = (1/\sqrt{2})(|1, 0, 0\rangle + |0, 0, 1\rangle)$, the first excited state is $|\psi_3\rangle_{\gamma\to\infty} = |0, 1, 0\rangle$ and the second excited state is $|\psi_1\rangle_{\gamma\to\infty} = (1/\sqrt{2})(|1, 0, 0\rangle - |0, 0, 1\rangle)$.

The situation for $\gamma < 0$ is very different and actually richer at the ground-state level. For $\gamma = -1$ we have a crossing in the single-particle spectrum, which therefore should have important consequences at the many-body level. At $\gamma = -1$ the ground state is two-fold degenerate between states $|\psi_1\rangle$ and $|\psi_2\rangle_{\gamma=-1}$. This manifold is also

spanned by so called semifluxon states, with π-flux and clockwise and counter-clockwise rotation [25],

$$\left|\psi_{\mathrm{sf1}}\right\rangle = \frac{1}{\sqrt{3}}\left(\mathrm{e}^{\mathrm{i}\frac{\pi}{3}}\left|1, 0, 0\right\rangle + \left|0, 1, 0\right\rangle + \mathrm{e}^{-\mathrm{i}\frac{\pi}{3}}\left|0, 0, 1\right\rangle\right)$$

$$\left|\psi_{\mathrm{sf2}}\right\rangle = \frac{1}{\sqrt{3}}\left(e^{-\mathrm{i}\frac{\pi}{3}}\left|1, 0, 0\right\rangle + \left|0, 1, 0\right\rangle + \mathrm{e}^{\mathrm{i}\frac{\pi}{3}}\left|0, 0, 1\right\rangle\right). \tag{7}$$

The first excited state is $|\psi_3\rangle_{\gamma=-1} = (|1, 0, 0\rangle - |0, 1, 0\rangle + |0, 0, 1\rangle)/\sqrt{3}$.

From figure 2, one can see that the main effect of varying γ is a large avoided crossing of the asymptotic states $(|1, 0, 0\rangle + |0, 0, 1\rangle)/\sqrt{2}$ and $|0, 1, 0\rangle$. When γ is positive the ground state is $(|1, 0, 0\rangle + |0, 0, 1\rangle)/\sqrt{2}$, whereas when γ is negative the lowest state is the state, $|\psi_1\rangle = (|1, 0, 0\rangle - |0, 0, 1\rangle)/\sqrt{2}$. The latter remains uncoupled for all values of γ, with eigenenergy $E = J\gamma$. This value is easy to obtain, since in the Fock basis: $[a_1^\dagger a_3 + a_3^\dagger a_1]|\psi_1\rangle = -|\psi_1\rangle$. Therefore, $\langle\psi_1| - J\gamma\left(a_1^\dagger a_3 + a_3^\dagger a_1\right)|\psi_1\rangle = J\gamma$.

2.1.2. Explicit symmetry breaking, effect of the bias

The explicit symmetry breaking induced by bias terms in the Hamiltonian (2) breaks the degeneracies present in the single-particle spectrum. As seen in figure 2, the crossings at $\gamma = -1$ and $\gamma = 1$, which occur in the non-interacting system for the ground state and excited states, respectively, become now avoided crossings. For the case we are interested in, when the bias is much smaller than the tunnelling, we can obtain the states dressed by the bias at the degeneracy points by means of first order perturbation theory. In the case of $\epsilon_{13} > 0$ and $\epsilon_{23} = 0$, the ground-state manifold at $\gamma = -1$ splits, $\Delta E = \epsilon_{13}$, and the corresponding dressed states are,

$$\left|\tilde\psi_1\right\rangle = \frac{1}{\sqrt{2}}\left(\left|\psi_2\right\rangle - \left|\psi_1\right\rangle\right)$$
$$= \frac{1}{\sqrt{12}}\left[\left(1 - \sqrt{3}\right)|1, 0, 0\rangle + 2\left|0, 1, 0\right\rangle + \left(1 + \sqrt{3}\right)|0, 0, 1\rangle\right].$$
$$\left|\tilde\psi_2\right\rangle = \frac{1}{\sqrt{2}}\left(\left|\psi_1\right\rangle + \left|\psi_2\right\rangle\right)$$
$$= \frac{1}{\sqrt{12}}\left[\left(1 + \sqrt{3}\right)|1, 0, 0\rangle + 2\left|0, 1, 0\right\rangle + \left(1 - \sqrt{3}\right)|0, 0, 1\rangle\right]. \tag{8}$$

The first one is the new ground state of the system, which has a slightly larger population of particles in site 3. This result is reasonable, since the bias we have considered, $\epsilon_{13} > 0$, promotes site 3.

From now on we have set the bias terms to $\epsilon_{13} = \epsilon_{23} \simeq 10^{-9}$ J. Their effect is not appreciable in any of the reported results.

2.2. Many-body basis

The system is studied through direct diagonalization of the many-body Hamiltonian for a fixed number of atoms, N. A suitable many-body basis is the Fock one, which labels the number of atoms in each mode,

$$|n_1, n_2, n_3\rangle = \frac{1}{\sqrt{n_1! \, n_2! \, n_3!}}\left(\hat{a}_1^\dagger\right)^{n_1}\left(\hat{a}_2^\dagger\right)^{n_2}\left(\hat{a}_3^\dagger\right)^{n_3}\,|\mathrm{vac}\rangle, \tag{9}$$

where $|\mathrm{vac}\rangle$ stands for the vacuum, and $N = n_1 + n_2 + n_3$. The elements of the Fock basis can be expressed as a product state $|n_1, n_2, n_3\rangle = |n_1\rangle \otimes |n_2\rangle \otimes |n_3\rangle$. A general many-body wavefunction is thus written as

$$|\Psi\rangle = \sum_{n_1, n_2}^{N} C_{n_1, n_2} |n_1, n_2, n_3\rangle, \tag{10}$$

where C_{n_1, n_2} is the corresponding amplitude of the Fock state $|n_1, n_2, n_3\rangle$, with $n_1 = 0, ..., N$; $n_2 = 0, ..., N - n_1$ and $n_3 = N - (n_1 + n_2)$.

2.3. Coherent states

Coherent states are the closest analogs to classical solutions, in the same way wavepackets are the closest quantum analog to classical trajectories. A general coherent state can be constructed by assuming that all N atoms populate the same single-particle state ℓ,

$$\hat{b}_\ell^\dagger \equiv c_1\,\hat{a}_1^\dagger + c_2\,\hat{a}_2^\dagger + c_3\,\hat{a}_3^\dagger. \tag{11}$$

The coherent state reads,

$$|\Psi_{\mathrm{COH}}\rangle = \frac{1}{\sqrt{N!}}\left(\hat{b}_\ell^\dagger\right)^N|\mathrm{vac}\rangle. \tag{12}$$

Since $c_i \in \mathbb{C}$, this many-body state has six parameters to be determined. Properly normalizing the single-particle wavefunction and also realizing that there is always an arbitrary global phase, the number of free parameters can be reduced to 4. It is worth stressing that a coherent state as the one defined above corresponds to a fully condensed atomic cloud.

2.4. Condensed fractions

The fragmentation properties of the ultracold atomic gas [2] can be investigated by means of the eigenvalues of the one-body density matrix. In our system with N bosons and three different modes, the one-body density matrix of a many-body state $|\Psi\rangle$ is a 3×3 matrix whose elements are,

$$\hat{\rho}_{ij}^{(1)} = \frac{1}{N}\left\langle \Psi \left| \hat{a}_i^\dagger \hat{a}_j \right| \Psi \right\rangle, \tag{13}$$

with $i, j = 1, 2, 3$. Since $|\Psi\rangle$ is normalized, it follows that $\mathrm{Tr}\ \hat{\rho}^{(1)} = 1$.

It is interesting to calculate its eigenvectors (natural orbitals), $|\psi_i\rangle$, and eigenvalues, p_i, with $p_1 \geqslant p_2 \geqslant p_3 \geqslant 0$, that satisfy $p_1 + p_2 + p_3 = 1$. Each eigenvalue of the one-body density matrix gives the relative occupation number of the corresponding natural orbital: $p_i = N_i/N$. In a singly condensed system, there is only one large eigenvalue that corresponds to the condensed fraction of the single-particle state, $|\psi_1\rangle$: $p_1 \sim 1$ and $N_1 \sim \mathcal{O}(N)$, with all the other eigenvalues p_j ($j \neq 1$) being small $\sim \mathcal{O}(1/N)$. Instead a fragmented system has more than one large eigenvalue, $N_i \sim \mathcal{O}(N)$, with $i = 1, ..., s$, and the rest of eigenvalues p_j ($j > s$) are small $\sim \mathcal{O}(1/N)$. In this situation the system is not fully condensed, but fragmented, quantum correlations become important and the mean-field approximation fails to describe the system.

2.5. Entanglement properties: entanglement entropy and Schmidt gap

Correlations between different subsystems of a many-body quantum system can be quantified performing different bipartite splittings. That is, considering the system as made of two subsystems, tracing out one of the parts, and studying the von Neumann entropy and the entanglement spectrum [27] of the resulting subsystem.

In our case, we consider different spatial partitions of the three-well configuration, e.g. (1,23), (2,13), as in [19]. From the density matrix of the full system, $\hat{\rho}$, correlations between mode i and the rest can be determined by first taking the partial trace of $\hat{\rho}$ over the Fock-state basis of the other modes. This yields the reduced density matrix on subsystem i, $\hat{\rho}_i$, that describes the state of this subsystem. For instance, in our system, by tracing out sites 2 and 3, a bipartite splitting of the three-mode system is obtained (1, 23), and the reduced density matrix on site 1, $\hat{\rho}_1 = \mathrm{Tr}_{2,3}\hat{\rho}$, is found to be diagonal in the single mode space of N particles (see equation (A.2) in the appendix),

$$\hat{\rho}_1 = \sum_{k=0}^{N} \lambda_k^{(1)}\ |k\rangle\langle k|, \quad \lambda_k^{(1)} \geqslant 0, \tag{14}$$

where $|k\rangle$ are states of k particles in mode 1. Note, that the reduced density matrix for state 1 is in general a mixture without a well-defined number of particles. The set of eigenvalues $\{\lambda_k^{(1)}\}$ is called entanglement, or Schmidt spectrum [27, 28] [5], and the eigenvalues are the Schmidt coefficients. The Schmidt coefficient $\lambda_k^{(1)}$ is in this case directly the probability of finding k particles in site 1 without measuring the number of atoms in sites 2 and 3. The Schmidt spectrum fulfills $\sum_i \lambda_i^{(1)} = 1$, and contains information about the correlations and the entanglement properties of the state in subsystem 1 with respect to the rest of the system. It is worth recalling that a many-body state is entangled when it cannot be written as a product state. In the case of spatially separated modes, the entanglement we are discussing is spatial.

A measure of the entanglement between the two subsystems is already provided by the single-site von Neumann entropy, which can be calculated as $S_1 = -\mathrm{Tr}(\hat{\rho}_1 \log \hat{\rho}_1)$. Noting that in our case the density matrix, $\hat{\rho}_1$, is already diagonal, see equation (14), the entropy can be evaluated from the Schmidt coefficients as $S_1 = -\sum_i \lambda_i^{(1)} \log \lambda_i^{(1)}$.

In the three-mode system, a signature of the entanglement on the Schmidt spectrum is the following one: if site 1 is not entangled with sites 2 and 3, it should be pure after tracing those sites out, and then the entanglement spectrum would only have one non-zero Schmidt coefficient. This actually implies a zero of the corresponding von Neumann entropy. A remarkable magnitude defined from the set of λ's is the so-called Schmidt gap, defined as the difference between the two largest and more relevant Schmidt coefficients in the entanglement spectrum of subsystem i, $\Delta\lambda^{(i)}$ [28]. In the case of no entanglement between the subsystems, the Schmidt gap takes its maximum value of 1. A vanishing of the Schmidt gap marks large entanglement between the subsystems. As has

---

[5] In our paper we adopt the definition of entanglement spectrum used in [28]. In [27], the entanglement spectrum is defined as $-\log(\lambda_i)$, whose interpretation is analogous to energy spectrum: the most occupied states are the low-lying ones in the entanglement spectrum.

been recently pointed out in [19] for dipolar bosons in triple-well potentials, the Schmidt gap is a good tool to distinguish between phase transitions and crossovers.

Note that no relation exists between fragmentation and entanglement, in the sense that a system can be entangled and fragmented independently. For instance, a system where all the bosons occupy the same spatial mode is nor fragmented neither spatially entangled. A bosonic Josephson junction in the strong repulsive interaction (Fock) regime is a clear example of a non entangled but fragmented state: $|N/2, N/2\rangle$. In contrast, in the non-interacting regime the bosonic Josephson junction is in a fully condensed state,

$$|\Psi\rangle = \frac{1}{\sqrt{N!}} \left(\frac{\hat{a}_1^\dagger + \hat{a}_2^\dagger}{\sqrt{2}} \right)^N |\text{vac}\rangle, \tag{15}$$

which has large entanglement between the two sites as seen by the Schmidt coefficients which are $\lambda_k = 2^{-N} \binom{N}{k}$. Finally, cat states, $|\Psi\rangle = (|N, 0\rangle + |0, N\rangle)/\sqrt{2}$, are a well known example of fragmented and entangled many-body states.

3. Quantum many-body properties of the system

We consider now the effect of repulsive interactions between atoms. We calculate the ground state, by exact diagonalization of the Hamiltonian, for different values of the tunnelling rate γ. In our numerics we will consider up to $N = 48$ particles. The ground state of the system is characterized by means of, (a) coherence properties and fragmentation, (b) analysis of the lower energy gaps, and (c) entanglement spectrum and entanglement entropy.

3.1. Analytic results in the $|\gamma| \gg 1$ limit

The structure of the single-particle spectrum, see figure 2, allows one to build a simple model for $|\gamma| \gg 1$. This simple model will serve as guidance to understand many of the properties of the many-body ground state which will be discussed in the forthcoming sections.

We can distinguish two distinct regimes, $\gamma \gg 1$ and $-\gamma \gg 1$. In both cases, for sufficiently large values of $|\gamma|$ the single-particle spectrum of equation (3) approaches $-|\gamma|J, 0$, and $|\gamma|J$. When $\gamma \gg 1$, the corresponding non-interacting single-particle states are $|\psi_2\rangle, |\psi_3\rangle$ and $|\psi_1\rangle$, respectively. When $-\gamma \gg 1$ we have $|\psi_1\rangle, |\psi_3\rangle$ and $|\psi_2\rangle$, respectively. For interaction strengths such that $NU/J \ll |\gamma|$, the effect of the interaction can be considered perturbatively. In this limit we can ignore particle-hole excitations to the highest single-particle state, and write configurations with k excited atoms as,

$$|\Psi\rangle = \mathcal{N} \left(\hat{a}_{\psi_2}^\dagger \right)^{N-k} \left(\hat{a}_{\psi_3}^\dagger \right)^k |\text{vac}\rangle \qquad \text{if } \gamma \gg 1,$$

$$|\Psi\rangle = \mathcal{N} \left(\hat{a}_{\psi_1}^\dagger \right)^{N-k} \left(\hat{a}_{\psi_3}^\dagger \right)^k |\text{vac}\rangle \qquad \text{if } -\gamma \gg 1, \tag{16}$$

where $\mathcal{N}$ is a normalization constant and $\hat{a}_{\psi_i}^\dagger$ creates a particle in the single-particle state $|\psi_i\rangle$. The energy for this state, up to constant terms, reads,

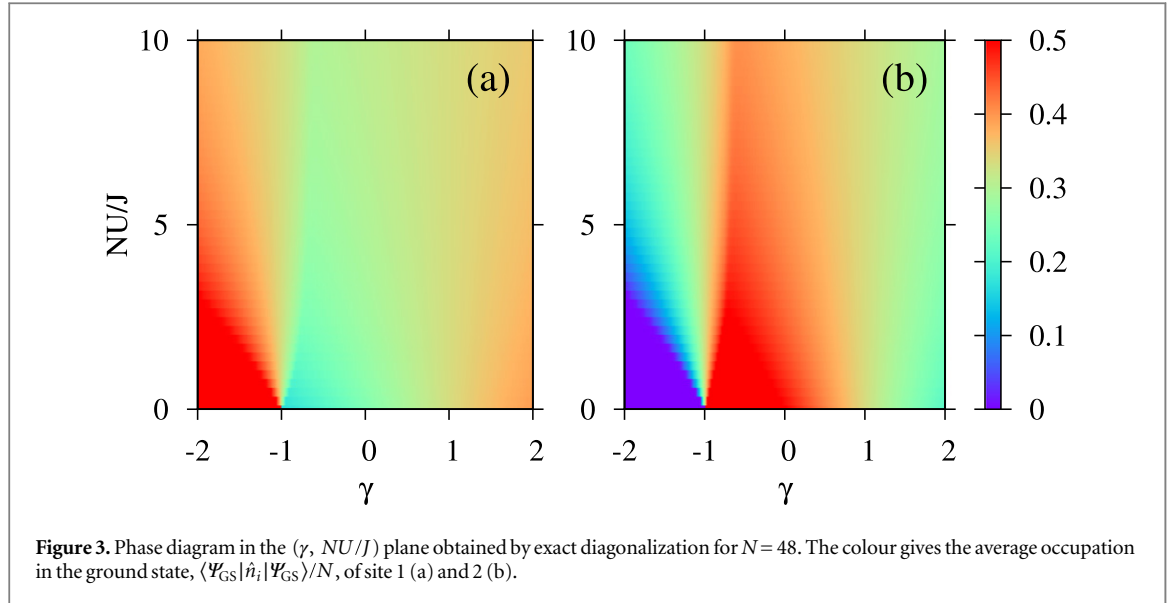$$E(N, k) = U \frac{N-k}{2} \left(\frac{N-k-1}{2} \right) + \frac{U}{2} k(k-1) + |\gamma| Jk. \tag{17}$$

In the non-interacting case, the energy is minimal for $k = 0$, as expected. Incidentally, for large interactions, $NU/J \gg 1$ (with $|\gamma|J \gg U$), the minimal energy is obtained for $k = N/3$, as expected for a Mott insulator of filling $N/3$. As we decrease interactions, the system goes step by step to $k = 0$. In particular, many-body states with k and $k + 1$ excited atoms degenerate if,

$$\frac{NU}{J} = \frac{2N|\gamma|}{N - 3k - 1}. \tag{18}$$

In this limit, it is quite reasonable to expect that as we increase the atom–atom interactions keeping γ fixed, the system tends to minimize the number of pairs per site, which is achieved by equipopulating the three sites. Equation (18) predicts ground state degeneracies, i.e. energy crossings, for certain values of $|\gamma|$ and NU/J.

This model works reasonably well both for $\gamma \lesssim -1$ and $\gamma \gtrsim 1$, where already the structure of the single-particle spectrum starts to resemble the asymptotic one. There is one important difference between $\gamma \lesssim -1$ and $\gamma \gtrsim 1$. In the former case, the lowest energy single-particle state is independent of γ (see figure 2) and has no population of site 2. This makes the model outlined above fairly accurate to describe the different transitions in the many-body ground state. In the latter however, the lowest single-particle state only asymptotically approaches the state $(1/\sqrt{2})(|1, 0, 0\rangle + |0, 0, 1\rangle)$. In this case, the model only provides a qualitative picture at smaller values of $|\gamma|$. Note also, that for $|\gamma| \gg 1$, the value of k which minimizes the energy, corresponds in this

Figure 3. Phase diagram in the $(\gamma, NU/J)$ plane obtained by exact diagonalization for $N = 48$. The colour gives the average occupation in the ground state, $\langle \Psi_{GS} | \hat{n}_i | \Psi_{GS} \rangle / N$, of site 1 (a) and 2 (b).

limit to the average population of site 2 in the ground state, while the average population of sites 1 and 3 is $(N - k)/2$.

3.2. Coherence and one-body density matrix

To have an overall picture of the different regimes that we will encounter for different values of NU/J and γ we first study the average populations of the three sites. Notice that in our system, without bias terms, sites 1 and 3 are equivalent. In figure 3 we present results for $-2 \leqslant \gamma \leqslant 2$ and relatively small values of the interaction $NU/J \leqslant 10$, which do not reach the Fock regime. For very small values of the dimensionless parameter NU/J, one does not expect sizeable changes from the single-particle case. Indeed in the ground state for $\gamma > -1$ the three modes are substantially populated, whereas for $\gamma < -1$ the second mode is clearly less occupied than the other two as reflected in the dark region in the left corner of figure 3(b).

In the non-interacting limit, $U = 0$, the problem becomes a single-particle one and in the case of a symmetric configuration, $\gamma = 1$, the many-body ground state can be written as [11, 29],
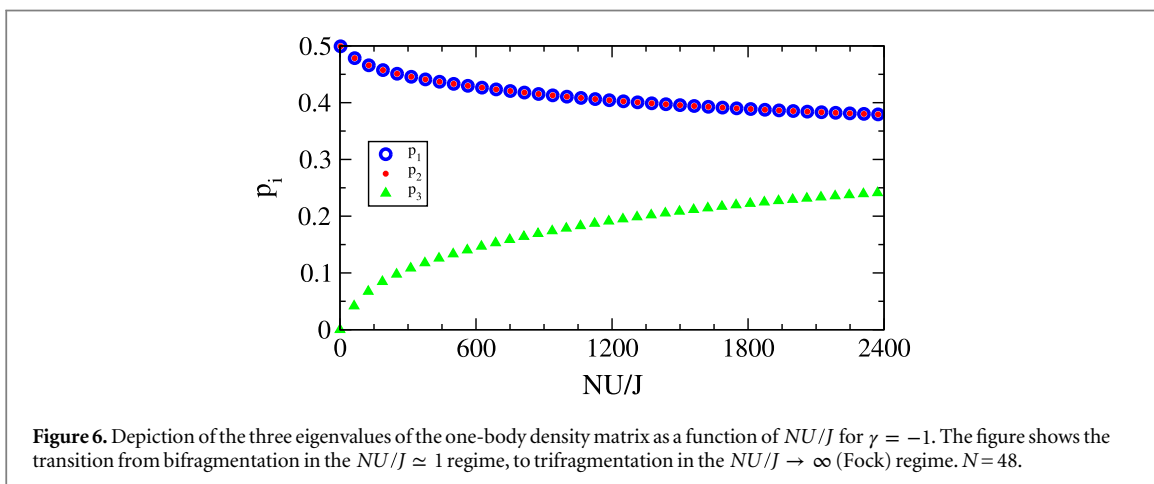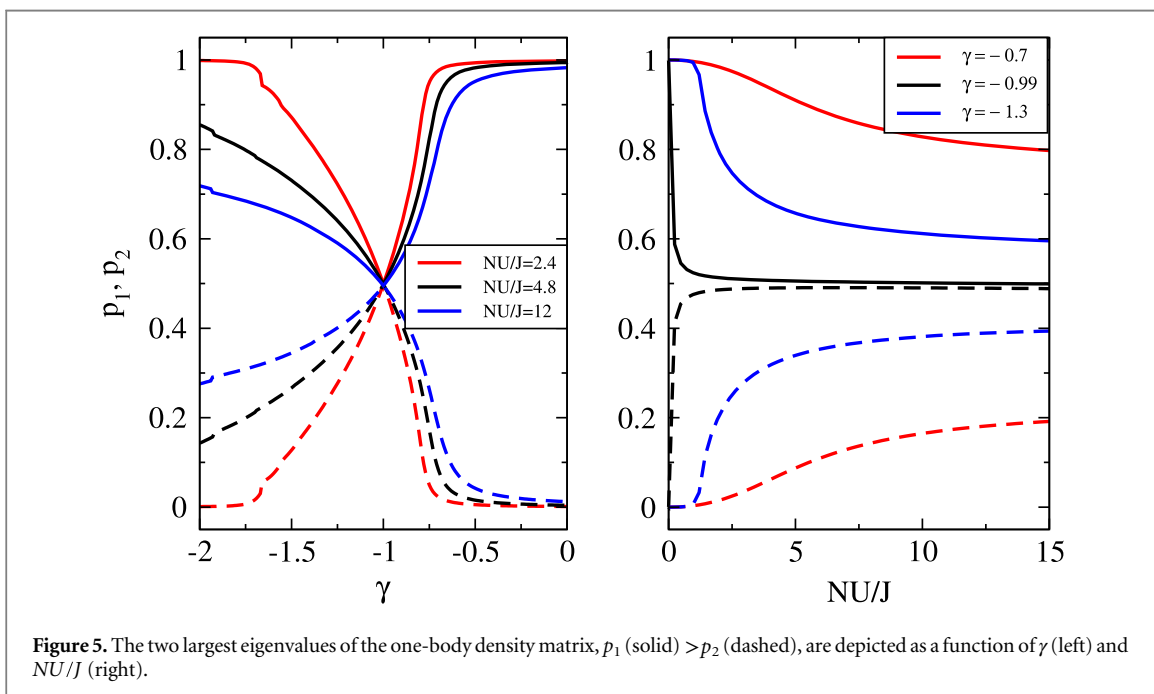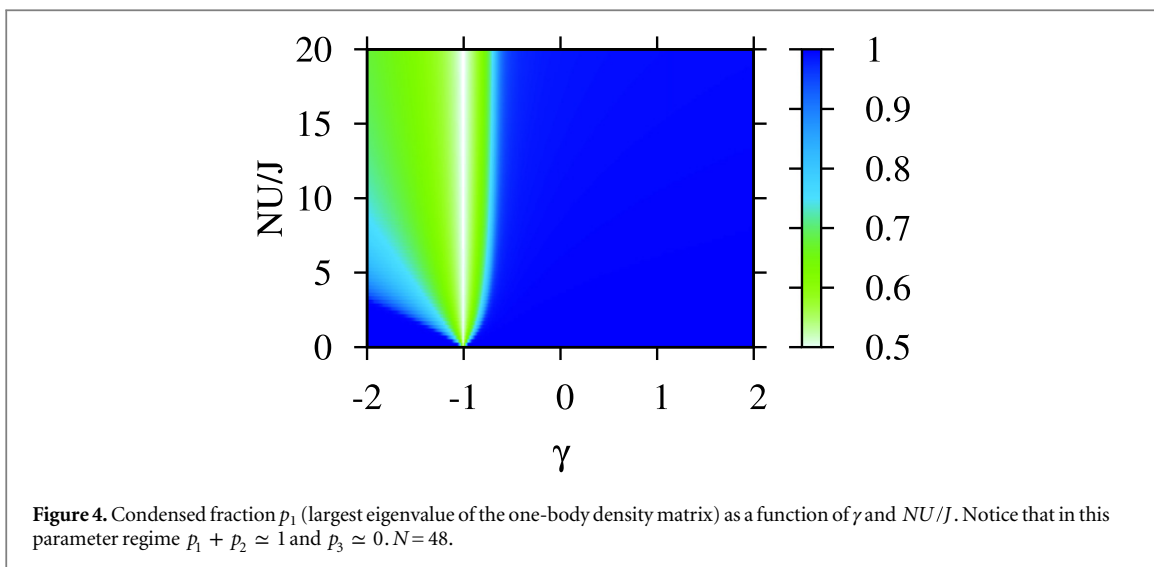
$$| \Psi_{GS}^{U=0} \rangle = \frac{1}{\sqrt{N!}} \left(\frac{1}{\sqrt{3}} \left[\hat{a}_1^\dagger + \hat{a}_2^\dagger + \hat{a}_3^\dagger \right] \right)^N |\text{vac}\rangle, \tag{19}$$
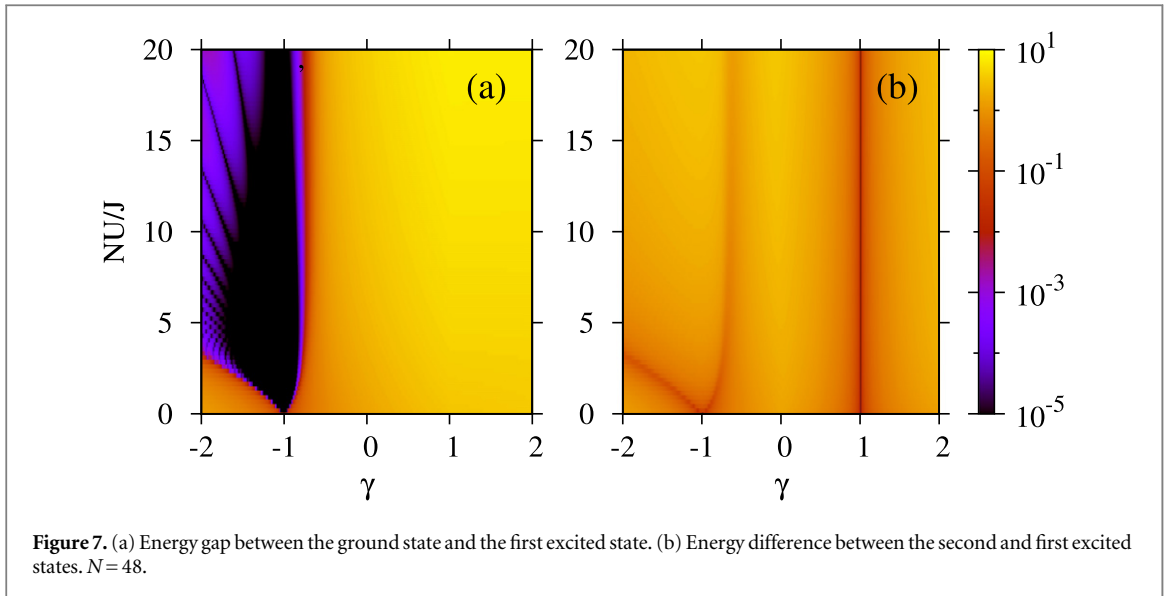
in which the average population on each site is, for symmetry reasons, $N/3$.

For large repulsive atom–atom interactions, regardless of the value of γ, the system will fragment in an effort to diminish the number of pairs inside each site, in analogy to, for instance, the double-well [2]. In the large interaction limit, that is in the Fock regime $U \gg J$, if the number of bosons is commensurate with 3, the ground state can be well approximated by $| \Psi_{GS}^{U \gg J} \rangle \simeq |N/3, N/3, N/3\rangle$, which is the equivalent to a Mott insulator of filling $N/3$. If the number of bosons is not proportional to 3 the ground state becomes three-fold degenerate in the strong Fock regime: $|N/3 \pm 1, N/3, N/3\rangle$, $|N/3, N/3 \pm 1, N/3\rangle$, and $|N/3, N/3, N/3 \pm 1\rangle$, where the plus (minus) sign refers to a single particle (hole) delocalization.

In the Josephson regime, defined as $NU/J \simeq 1$, the ground state of the system is mostly condensed for $\gamma \gtrsim -0.5$. This is reflected in the eigenvalues of the one-body density matrix, see figure 4 and left panel in figure 5. As already pointed out in the single-particle spectrum, a very interesting feature is readily found in the vicinity of $\gamma = -1$. In this case, the ground state of the system is fragmented in two pieces even in the non-interacting case. As the interaction increases, but still in the Josephson regime, the system is seen to remain bifragmented. From figure 5, one can see that the region in the γ-space, around $\gamma = -1$, which corresponds to a fragmented condensate, slightly expands with the interaction.

As discussed above, in the limit of the strong Fock regime, the ground state should be essentially fragmented in three pieces (in our case $N = 48$, which is multiple of 3), corresponding to the ground state $|N/3, N/3, N/3\rangle$. This is clearly seen in figure 6, which depicts the behavior of the three eigenvalues of the one-body density matrix in the $\gamma = -1$ configuration for different values of the interaction. In the non-interacting case, the system is fragmented in two condensates ($p_1 = p_2 = 0.5$ and $p_3 = 0$), whereas as NU/J increases, $p_1 = p_2 < 0.5$ decrease and $p_3 > 0$ increases, fulfilling $p_1 + p_2 + p_3 = 1$. Moreover, one can see that $p_i \to 1/3$ asymptotically. Note however that the origin of bifragmentation is directly related to the degeneracy at the single-particle level and

Figure 4. Condensed fraction p_1 (largest eigenvalue of the one-body density matrix) as a function of γ and NU/J. Notice that in this parameter regime $p_1 + p_2 \simeq 1$ and $p_3 \simeq 0$. $N = 48$.

Figure 5. The two largest eigenvalues of the one-body density matrix, p_1 (solid) $> p_2$ (dashed), are depicted as a function of γ (left) and NU/J (right).

Figure 6. Depiction of the three eigenvalues of the one-body density matrix as a function of NU/J for $\gamma = -1$. The figure shows the transition from bifragmentation in the $NU/J \simeq 1$ regime, to trifragmentation in the $NU/J \to \infty$ (Fock) regime. $N = 48$.

Figure 7. (a) Energy gap between the ground state and the first excited state. (b) Energy difference between the second and first excited states. $N = 48$.

remains in the presence of tunnelling. Trifragmentation requires strong interactions such that essentially tunnelling plays no role and the system can be regarded as three independent condensates.

In the right panel of figure 5 the behavior of the two largest eigenvalues of the one-body density matrix is shown, as a function of NU/J, for a fixed γ configuration. At $\gamma = -0.99$ there is a sharp transition from a singly condensed (at $U = 0$) to a bifragmented system already for very small values $NU/J > 0$. However, as γ departs further from -1 ($\gamma = -0.7$ and -1.3) the transition between both regimes becomes smoother, and the system remains fully condensed for a larger range of interactions.

It is worth emphasizing that the quantum phase transition from superfluid to Mott insulator transition, i.e. from fully condensed to trifragmented, occurs for $\gamma \neq -1$. For $\gamma = -1$ the quantum phase transition takes place between a bifragmented phase and the Mott insulator, as discussed above.

3.3. Energy spectrum

The model presented in section 3.1 predicts a number of degeneracies in the many-body energy spectrum of the system. Indeed, equation (18) predicts $N/3$ energy crossings for both $\gamma < -1$ and $\gamma > 1$. As explained above, these predictions are expected to hold for $\gamma \lesssim -1$ and are indeed found in the exact many-body spectrum as seen in figure 7. Varying the value of k in equation (18) from 0 to $N/3$ one obtains the large $|\gamma|$ behavior of the different lines of zero gap in figure 7 (a). Similarly, albeit not shown in the figure, for $\gamma \gg 1$ the corresponding gapless lines are also found in the system.

For $\gamma > 0$, also interesting is the closing of the energy gap between the first and second excited states for $\gamma = 1$ (see the vertical line in the right panel of figure 7). It corresponds to the degeneracy between vortex and antivortex states studied in [11], whose wavefunctions have been previously obtained in the non-interacting case, see equation (5). As the interaction is increased the degeneracy between the corresponding two states remains.

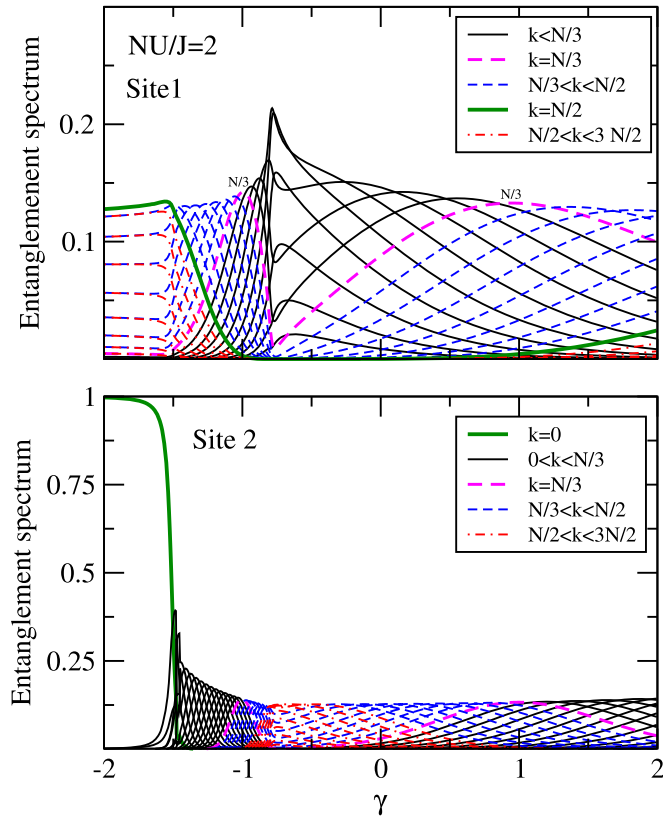### 3.4. Entanglement spectrum and entanglement entropy

The many-body ground state has been found to be fragmented in the vicinity of $\gamma = -1$ and mostly condensed otherwise, for $NU/J \simeq 1$. Besides fragmentation, the three-site configuration considered allows one to study the onset of entanglement and correlations among the three different sites depending on the specific values of the parameters. To characterize the spatial entanglement properties we will use the Schmidt gap and the entanglement von Neumann entropy defined in section 2.5.

Due to the structure of our system, with three sites where two of them, 1 and 3, are essentially equivalent, one can consider two bipartite splittings. The first one corresponds to subsystem 1 where sites 2 and 3 have been traced off (1, 23). And second, subsystem 2 where subsystems 1 and 3 have been traced off (2, 13).

The Schmidt gap corresponding to both bipartite splittings in the (γ, NU/J) diagram is presented in figure 8. The first notable feature is that in both bipartite splittings we observe two fan-like radial structures, with straight lines converging to $(-1, 0)$ and $(1, c)$ (with c a constant to be discussed later). This structure, similar to the one discussed in [19], represents the crossings of the first two values of the entanglement spectrum. To better understand the structure, in figure 9 we plot the entanglement spectrum ($N + 1$ coefficients) for both bipartite splittings for a fixed value of $NU/J = 2$. For $\gamma < -1$, each zero of the Schmidt gap shown in figure 8 implies a
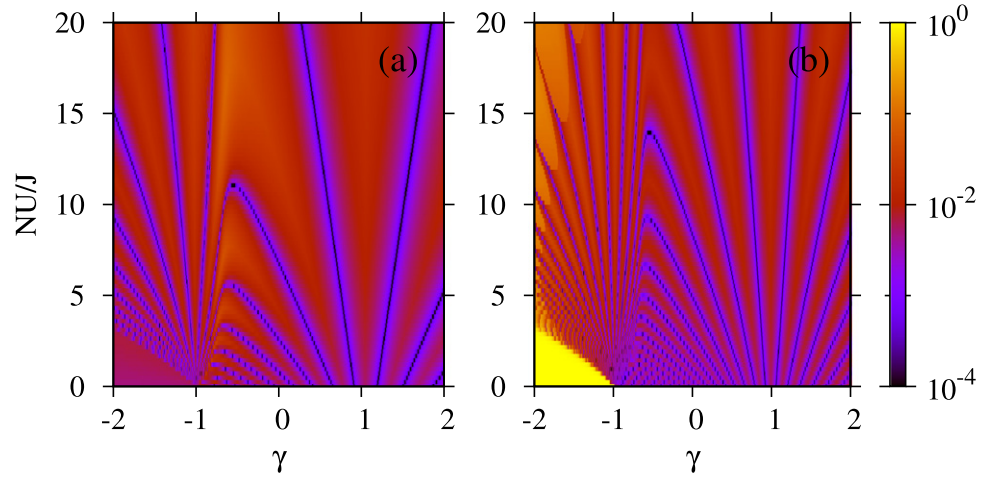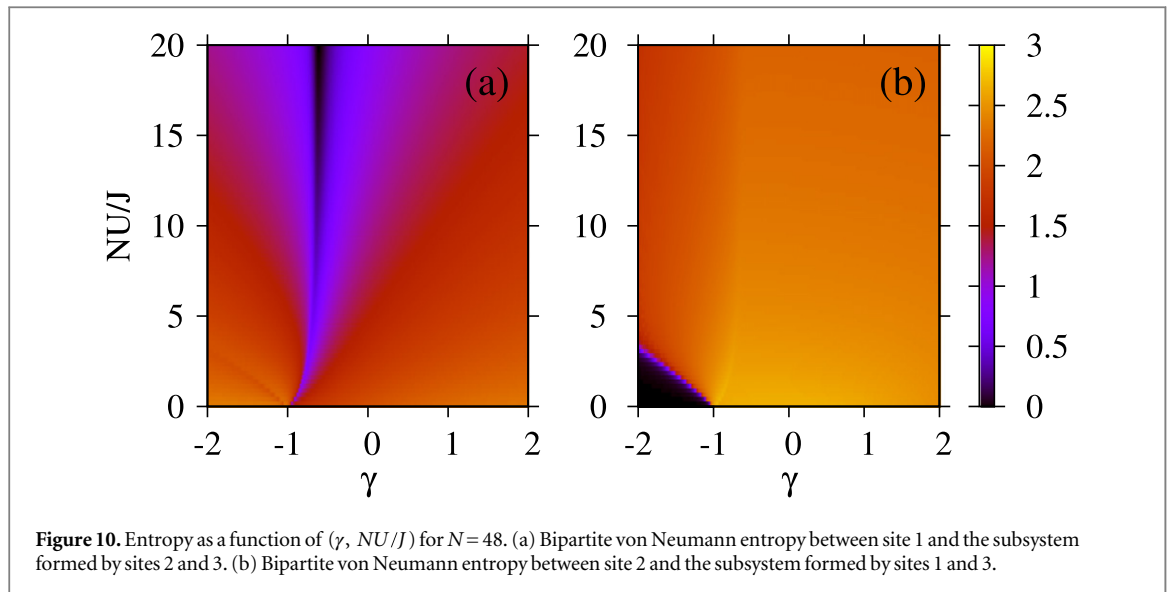
Figure 8. Schmidt gap as a function of (γ, NU/J) for $N = 48$. (a) Between site 1 and the subsystem formed by sites 2 and 3. (b) Between site 2 and the subsystem formed by sites 1 and 3.

Figure 9. Entanglement spectrum of the reduced density matrix of mode 1 and mode 2, upper and lower panel, respectively. Upper panel, $\lambda_k^{(1)}$, $k = 1, ..., N/3$ (solid lines), $k = N/3$ (thick dashed line), $N/3 < k < N/2$ (thin dashed lines), $k = N/2$ (thick solid line), and $N/2 < k < 3N/2$ (thin dotted–dashed lines). Lower panel, $\lambda_k^{(2)}$, $k = 0$ (thick solid line), $0 < k < N/3$ (solid lines), $k = N/3$ (thick dashed line), $N/3 < k < N/2$ (thin dashed lines), $k = N/2$ (thick solid line), and $N/2 < k < 3N/2$ (thin dotted–dashed lines). Both are computed for $NU/J = 2$ and $N = 48$.

variation of one unit of the most probable population of the untraced mode. This can be understood from the expression in equation (A.2), where the reduced density matrix is shown to be diagonal in the Fock basis of the untraced mode.

The simple large $|\gamma|$ model described in section 3.1 also explains qualitatively the observed behaviour. The degeneracies in the energy spectrum obtained there correspond to many-body ground states in which the most likely value of the population in site 2 goes from 0 to $N/3$ and the corresponding one of sites 1 and 3 from $N/2$ to

Figure 10. Entropy as a function of (γ, NU/J) for $N = 48$. (a) Bipartite von Neumann entropy between site 1 and the subsystem formed by sites 2 and 3. (b) Bipartite von Neumann entropy between site 2 and the subsystem formed by sites 1 and 3.

$N/3$. We have considered $N = 48$, see figure 8, and thus we find 16 crossings in the left part of the figure, with the most likely population of site 1 going from $N/2 = 24$ in the leftmost case to $N/3 = 16$ at $\gamma = -1$. As explained in the previous section, the perturbative model captures the physics also for $\gamma > 1$. As we can see in the figure, at $\gamma = 1$ the most likely population of site 1 is again $N/3 = 16$ and it keeps increasing as γ is increased.

These crossings described in the entanglement spectrum, clearly visible in figure 9, are one of the main signatures of a crossover between two phases, whereas in a quantum phase transition all the Schmidt coefficients degenerate to the same value in the thermodynamic limit ($N \to \infty$) [28]. In our case, it is clear that at ($\gamma = -1$, $NU/J \to 0$) all the Schmidt coefficients degenerate even for finite N. This is due to the fact that we already have a single-particle degeneracy.

Certain limiting cases are easily interpreted. For instance, for $\gamma \ll -1$, mode 2 is essentially unpopulated and decoupled from modes 1 and 3. This reflects in a singly populated entanglement spectrum for $NU/J = 2$ in figure 9 (lower panel). In this regime, the system was shown to be condensed in figure 5, on the single-particle state $(1, 0, -1) \equiv (|1, 0, 0\rangle - |0, 0, 1\rangle)/\sqrt{2}$, which spatially entangles modes 1 and 3, as seen in figure 9 (upper panel). In the $\gamma \gg 1$ limit the situation is similar, but as explained above, the $(1, 0, 1)$ limit is achieved in practice for much larger values of $|\gamma|$ than in the $\gamma < 0$ case. In both cases, the Schmidt spectrum is given by $\lambda_k = \binom{N}{k}/2^N$. In the vicinity of $\gamma = 0$ the three single-particle states quasidegenerate. This makes that for relatively low interactions, as in figure 9, the many-body ground state starts populating the Fock states around $N/3$ approaching the Mott insulator phase.
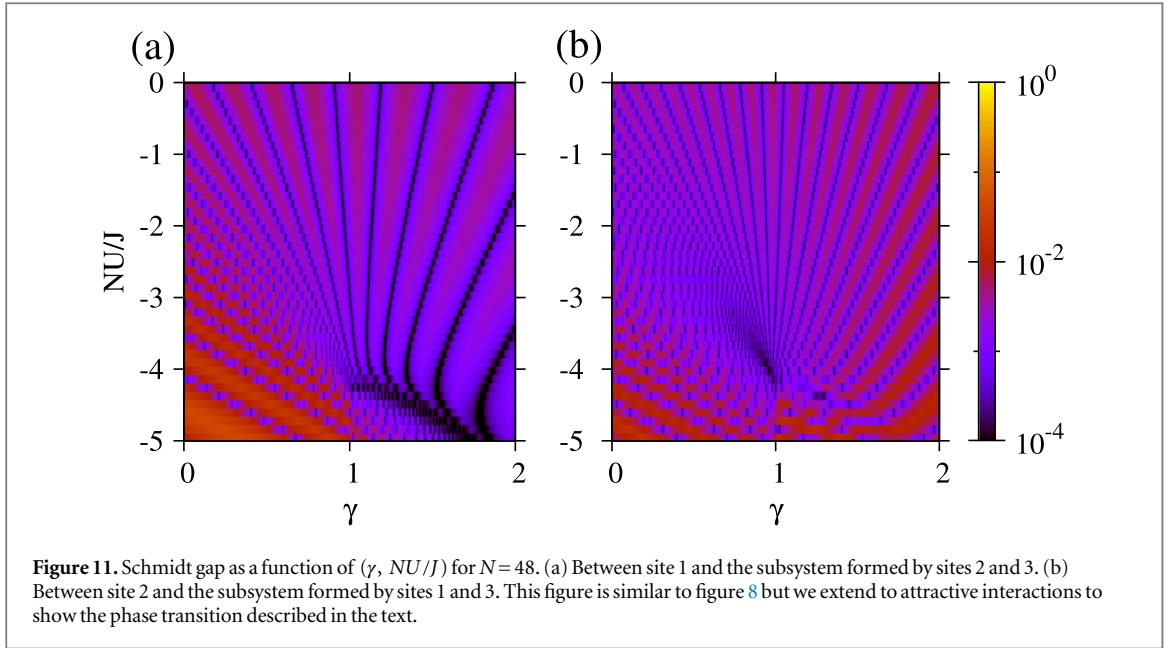
These features, described on the full entanglement spectrum, reflect directly on the corresponding von Neumann entropies, see figure 10. For instance, the fact that the system approaches the Mott regime for relatively low values of the interaction in the vicinity of $\gamma = 0$ reflects in an almost zero value of the von Neumann entropy for mode 1, which starts to decouple from the other modes. For $\gamma < -1$ and small values of the interaction, the system empties mode 2 and decouples it from the other two modes, see figure 10 (right panel).

3.5. Phase transition for attractive interactions

Similarly to the two-well system, a phase transition can be expected for $\gamma = 1$ for attractive interactions [33, 34]. In this case, the three sites are completely equivalent. Increasing the attractive atom–atom interactions, the system will minimize energy by clustering the atoms in a single site. In absence of any spatial bias, the ground state of the system will approach the Schrödinger cat-like state,

$$|\Psi_{cs}\rangle = \frac{1}{\sqrt{3}}(|N, 0, 0\rangle + |0, N, 0\rangle + |0, 0, N\rangle). \qquad (20)$$

Analogously to the two-site case, this many-body state is not gapped and is quasidegenerate with its first two excitations. In the thermodynamic limit, the transition between the non-interacting state, equation (19), and the cat-like state equation (20) goes through a transition point at a finite value of NU/J. This transition reflects in the behaviour of the Schmidt gap of the system. As seen in figure 8, several zero-Schmidt-gap straight lines tend to converge on a point in the attractive interaction regime on the $\gamma = 1$ line. In figure 11 we extend the range of parameters to the attractive region and certainly the lines seem to converge at $\gamma = 1$ and $-9/2 < NU/J < -4$,

Figure 11. Schmidt gap as a function of $(\gamma, NU/J)$ for $N = 48$. (a) Between site 1 and the subsystem formed by sites 2 and 3. (b) Between site 2 and the subsystem formed by sites 1 and 3. This figure is similar to figure 8 but we extend to attractive interactions to show the phase transition described in the text.

which is where the authors of [15, 18] predicted the existence of a self-trapping transition. Notably, in contrast with the former phase transition described at $\gamma = -1$, this phase transition is only present in the thermodynamic limit.

3.6. Detailed analysis of the $\gamma = -1$ case

The $\gamma = -1$ case is equivalent, related by a local gauge transformation, to the π-flux case discussed in [10, 15]. We will use similar techniques to those in [10] to build an approximate model to understand the fragmentation for small interaction energies.

As already shown in figures 5 and 6, the $\gamma = -1$ ground state is found to be bifragmented, with $p_1 = p_2 = 1/2$, in the non-interacting limit ($NU/J = 0$). To a good approximation it remains bifragmented for finite but small interactions ($NU/J \simeq 1$). As NU/J increases further the system approaches the Fock regime and the ground-state tends to the well known trifragmented configuration with $p_1 = p_2 = p_3 = 1/3$. We will here instead focus on the description of the special bifragmented states obtained when NU/J is non-vanishing but small.

At $\gamma = -1$ the single particle spectrum, see figure 2, has two degenerate eigenvalues, $E_{sf1} = E_{sf2} = -J$, and one excited state, $|e\rangle$, $E_e = 2J$. To understand the onset of bifragmentation we will now develop an approximate model in the following way: we neglect excitations away from the groundstate manifold spanned by the two semifluxon states, equation (7), whose creation operators are,

$$\hat{a}^\dagger_{sf1} = \frac{1}{\sqrt{3}} \left(e^{i\pi/3} \hat{a}^\dagger_1 + \hat{a}^\dagger_2 + e^{-i\pi/3} \hat{a}^\dagger_3 \right),$$

$$\hat{a}^\dagger_{sf2} = \frac{1}{\sqrt{3}} \left(e^{-i\pi/3} \hat{a}^\dagger_1 + \hat{a}^\dagger_2 + e^{i\pi/3} \hat{a}^\dagger_3 \right). \tag{21}$$

Then the interaction Hamiltonian in this subspace becomes [10]

$$\tilde{H}_U = \frac{U}{6} \left(\hat{N}^2_{sf1} + \hat{N}^2_{sf2} + 4\hat{N}_{sf1}\hat{N}_{sf2} - \hat{N}_{sf1} - \hat{N}_{sf2} \right), \tag{22}$$

where $\hat{N}_{sf1} = \hat{a}^\dagger_{sf1}\hat{a}_{sf1}$ and $\hat{N}_{sf2} = \hat{a}^\dagger_{sf2}\hat{a}_{sf2}$. From equation (22) it is clear that the Fock states built from the new modes

$$|N_{sf1}, N_{sf2}\rangle \equiv \frac{1}{\sqrt{N_{sf1}!N_{sf2}!}} \left(\hat{a}^\dagger_{sf1} \right)^{N_{sf1}} \left(\hat{a}^\dagger_{sf2} \right)^{N_{sf2}} |vac\rangle \tag{23}$$

are the eigenvectors of $\tilde{H}_U$, with an obvious expression for the eigenvalues. Since $N_{sf1} + N_{sf2} = N$, it will be more clarifying to change notations to $N_{sf1} = k$ and $N_{sf2} = N - k$. Then the spectrum becomes

$$\tilde{E}_U(k) = \frac{U}{6} \left(k^2 + (N-k)^2 + 4k(N-k) - N \right), \tag{24}$$

which is degenerate in pairs, $(k, N - k)$, except the topmost energy when N is even. In particular, the ground state is two-fold degenerate.
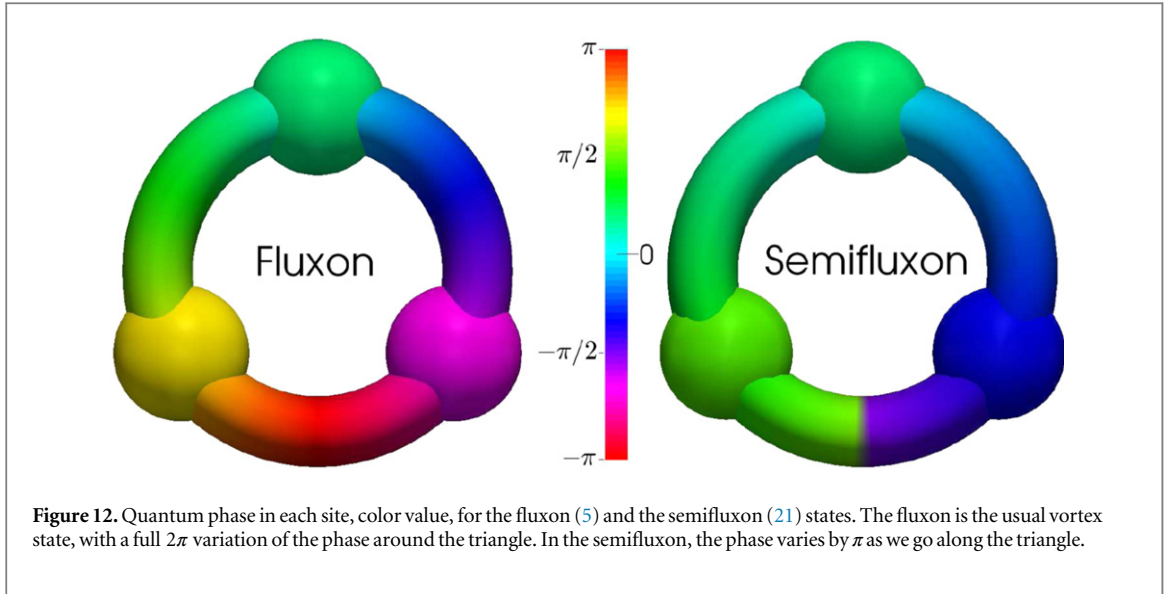
Figure 12. Quantum phase in each site, color value, for the fluxon (5) and the semifluxon (21) states. The fluxon is the usual vortex state, with a full 2π variation of the phase around the triangle. In the semifluxon, the phase varies by π as we go along the triangle.

This approximation turns out to be very accurate for small interactions. The effect of including the $|e\rangle$ state, breaks the degeneracy but does not promote any of the states. The lowest many body states are then well approximated by,

$$\left|\Psi_k^{(\pm)}\right\rangle = \frac{1}{\sqrt{2}}\left[|k, N - k\rangle \pm |N - k, k\rangle\right]$$
$$\text{with } k = 0, ..., N \tag{25}$$

where the $\pm$ sign labels the two states which would be degenerate in energy in absence of coupling with $|e\rangle$. The $|\Psi_k^{(\pm)}\rangle$ are obviously bifragmented, and have $p_1 = p_2 = 1/2$. Furthermore, the ground state is a cat-state with all atoms populating each of the semifluxon states in equation (21) [36].

As explained above, a semifluxon is a quantum state which carries half the quantum flux of the vortex states of equation (5). In our case, we have a discrete version, equation (7), as going around the triangle the quantum phase grows from 0 to π, with the phase jump of π imposed by $\gamma = -1$ configuration. In figure 12 we depict the phase structure of the discrete semifluxon state, compared to the usual vortex, equation (5) (referred to as 'fluxon').
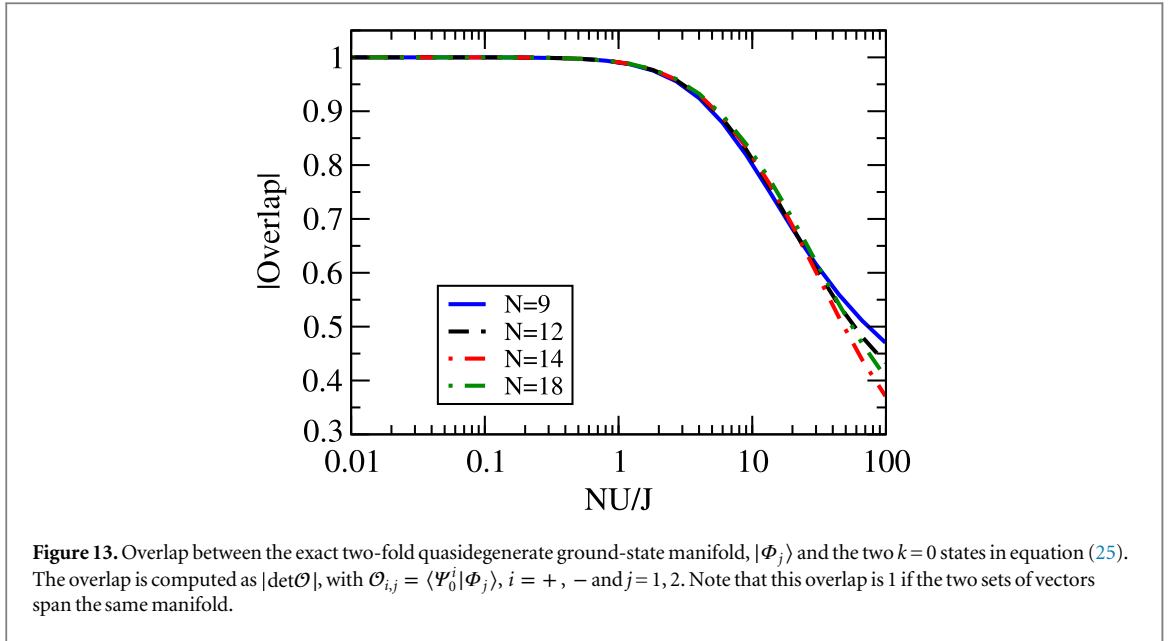
In the full three-mode space, as said above, the degeneracy of each doublet $|\Psi_k^{(\pm)}\rangle$, splits and therefore the ground state should be a NOON state of both semifluxon states. In figure 13 we depict the overlap of the exact ground state and first excited state with the corresponding $|\Psi_0^{(\pm)}\rangle$ states in equation (25). The model is seen to be fairly accurate up to $NU/J \simeq 10$. In an experimental measurement, one should thus find a fractional flux in one or the other direction in this interaction regime.

4. Summary and conclusions

A simple configuration consisting of three sites with a single tunable link has been shown to exhibit a large variety of quantum many-body properties. An important novelty of the proposed scheme is that we have considered cases in which the tunnelling rate in one of the links is tuneable, considering both zero-phase and π-phase tunnelling. In both cases, we have performed diagonalizations for finite number of particles, up to $N = 48$, and have examined the many-body properties of the system as a function of the atom–atom interaction and the tunable tunnelling rates.

By varying the tunnelling in one link, by means of the parameter γ, which is within reach experimentally as explained in the introduction, one explores configurations ranging from the colinear $\gamma = 0$, the fully symmetric $\gamma = 1$, to the symmetric π-phase, $\gamma = -1$. In the first two cases, the many-body ground state for small interactions $NU/J \sim 1$ is highly condensed, with one of the three eigenvalues of the one-body density matrix clearly scaling with the total number of particles. As we approach the $\gamma = -1$ point the system departs from condensation and becomes bifragmented for small interactions. This is partly a consequence of the degeneracy in the single-particle spectrum for $\gamma = -1$.

Two phase transitions are present in this system. The first takes place in the symmetric configuration $\gamma = 1$, but only for attractive interactions, which therefore makes it difficult to explore experimentally. This phase transition is reminiscent of the one present in other few-site models, e.g. bosonic Josephson junctions, and marks the transition to Schrödinger cat-like ground states in the spectrum [33–35]. Interestingly, for $\gamma = -1$ we find a second phase transition, which takes place in absence of interactions and which has clear consequences for

Figure 13. Overlap between the exact two-fold quasidegenerate ground-state manifold, $|\Phi_j\rangle$ and the two $k=0$ states in equation (25). The overlap is computed as $|\det \mathcal{O}|$, with $\mathcal{O}_{i,j} = \langle \Psi_0^i | \Phi_j \rangle$, $i = +, -$ and $j = 1, 2$. Note that this overlap is 1 if the two sets of vectors span the same manifold.

small repulsive atom–atom interactions. This phase transition has been characterized by the behaviour of the entanglement spectrum for the two possible independent bipartite splittings as we approach the transition point [28]. At the transition the entanglement spectrum degenerates and the corresponding von Neumann entropies exhibit a maximum. Interactions do not wash out the main features of this transition, which becomes essentially a crossover, which has clear consequences at finite interaction, such as the bifragmentation discussed above.

Finally, for the $\gamma = -1$ case and small interactions, the macroscopic superpositions of superfluid flows studied in [10] are described as macroscopic superpositions of discrete semifluxon states with opposite currents in the particular gauge we are implementing with a tunable link. A two-mode approximation has been shown to correctly describe both the fragmentation of the ground state and the low-energy excitations of the system.

Acknowledgments

Appendix. Diagonal structure of reduced density matrices

The many-body ground state of a BH Hamiltonian of N atoms in a triple-well potential, can be expressed as

$$|\Psi\rangle = \sum_{k,l} C_{k,l} \, |k, l, N - k - l\rangle,$$

where the Fock basis of the system can be written as a product state of the reduced Fock basis $\{|k\rangle_j\}$ for each subsystem $j = 1, 2, 3$:

$$|k, l, N - k - l\rangle = |k\rangle_1 \otimes |l\rangle_2 \otimes |N - k - l\rangle_3.$$

The reduced density matrix of subsystem 1 can be computed as

$$
\begin{aligned}
\hat{\rho}_1 &= \sum_{m,n} {}_2\langle m|_3 \langle n| \left(\sum_{k,l} C_{k,l} |k, l, N - k - l\rangle \sum_{k',l'} C_{k',l'}^* \langle k', l', N - k' - l'| \right) |m\rangle_2 |n\rangle_3, \\
&= \sum_{m,n} \sum_{k,k'} \sum_{l,l'} \delta_{l,m}\, \delta_{N-k-l,n}\, \delta_{N-k'-l',n}\, \delta_{l',m}\, C_{k',l'}^* C_{k,l} \,_1|k\rangle \langle k'|_1, \\
&= \sum_{k,m} \left| C_{k,m} \right|^2 |k\rangle \langle k|.
\end{aligned}
\tag{A.1}
$$

From this expression one can see that the reduced density matrix of one subsystem i is diagonal in the reduced Fock basis of the corresponding mode $\{|k\rangle\} \equiv \{|k\rangle_i\}$:

$$\hat{\rho}_i = \sum_{k=0}^{N} \lambda_k^{(i)} \, |k\rangle\langle k|, \tag{A.2}$$

with $\{\lambda_k^{(i)}\}$ the Schmidt coefficients that contain the information concerning the entanglement properties of subsystem i with the rest of the system.

References

[1] Dalfovo F, Giorgini S, Pitaevskii L and Stringari S 1999 *Mod. Phys. Rev.* **71** 463
[2] Mueller E J, Ho T L, Ueda M and Baym G 2006 *Phys. Rev.* A **74** 033612
[3] Albiez M, Gati R, Fölling J, Hunsmann S, Cristiani M and Oberthaler M K 2005 *Phys. Rev. Lett.* **95** 010402
[4] Levy S, Lahoud E, Shomroni I and Steinhauer J 2007 *Nature* **449** 579
[5] Gross C, Zibold T, Nicklas E, Estève J and Oberthaler M K 2010 *Nature* **464** 1165
[6] Riedel M F, Böhi P, Li Y, Hänsch T W, Sinatra A and Treutlein P 2010 *Nature* **464** 1170
[7] Nshii C C, Vangeleyn M, Cotter J P, Griffin P F, Hinds E A, Ironside C N, See P, Sinclair A G, Riis E, Arnold A S and 2013 *Nat. Nanotechnology* **8** 321
[8] Nemoto K, Holmes C A, Milburn G J and Munro W J 2000 *Phys. Rev.* A **63** 013604
[9] Paraoanu Gh S 2003 *Phys. Rev.* A **67** 023607
[10] Hallwood D W, Burnett J and Dunningham J 2006 *New J. Phys.* **8** 180
[11] Lee C, Alexander T J and Kivshar Y S 2006 *Phys. Rev. Lett.* **97** 180408
[12] Viscondi T F, Furuya K and de Oliveira M C 2010 *Europhys. Lett.* **90** 10014
[13] Franzosi R and Penna V 2003 *Phys. Rev.* E **67** 046227
[14] Viscondi T F and Furuya K 2011 *J. Phys. A: Math. Theor.* **44** 175301
[15] Arwas G, Vardi A and Cohen D 2014 *Phys. Rev.* A **89** 013601
[16] Lahaye T, Pfau T and Santos L 2010 *Phys. Rev. Lett.* **104** 170404
[17] Mazzarella G and Dell'Anna L 2013 *Eur. Phys. J. Spec. Top.* **217** 197
[18] Dell'Anna L, Mazzarella G, Penna V and Salasnich L 2013 *Phys. Rev.* A **87** 053620
[19] Gallemí A, Guilleumas M, Mayol R and Sanpera A 2013 *Phys. Rev.* A **88** 063645
[20] Xiong B and Fischer U R 2013 *Phys. Rev.* A **88** 063608
[21] Tarruell L, Greif D, Uehlinger T, Jotzu G and Esslinger T 2012 *Nature* **483** 302
[22] Eckardt A, Weiss C and Holthaus M 2005 *Phys. Rev. Lett.* **95** 260404
[23] Szirmai G, Mazzarella G and Salasnich L 2014 *Phys. Rev.* A. **90** 013607
[24] Jaksch D and Zoller P 2003 *New J. Phys.* **5** 56
[25] Goldobin E, Koelle D and Kleiner R 2002 *Phys. Rev.* B **66** 100508(R)
    Walser R, Schleich W P, Goldobin E, Crasser O, Koelle D and Kleiner R 2008 *New J. Phys.* **10** 045020
[26] Juliá-Díaz B, Martorell J and Polls A 2010 *Phys. Rev.* A. **81** 063625
[27] Li H and Haldane F D M 2008 *Phys. Rev. Lett.* **101** 010504
[28] de Chiara G, Lepori L, Lewenstein M and Sanpera A 2012 *Phys. Rev. Lett.* **109** 237208
[29] Casetti L and Penna V 2002 *J. Low Temp. Phys.* **126** 455
[30] Juliá-Díaz B, Zibold T, Oberthaler M K, Melé-Messeguer M, Martorell J and Polls A 2012 *Phys. Rev.* A **86** 023615
[31] Javanainen J and Ivanov M Y 1999 *Phys. Rev.* A **60** 2351
[32] Ziń P, Chwedeńczuk J, Oleś B, Sacha K and Trippenbach M 2008 *Europhys. Lett.* **83** 64007
[33] Cirac J I, Lewenstein M, Molmer K and Zoller P 1998 *Phys. Rev.* A **57** 1208
[34] Juliá-Díaz B, Dagnino D, Lewenstein M, Martorell J and Polls A 2010 *Phys. Rev.* A **81** 023615
[35] Raventós D, Graß T and Juliá-Díaz B 2014 arXiv:1410.7280
[36] Aghamalyan D, Cominotti M, Rizzi M, Rossini D, Hekking F, Minguzzi A, Kwek L-C and Amico L 2015 *New J. Phys.* **17** 045023